Motion control of linear induction motor using self-recurrent wavelet neural network trained by model predictive controller

Fatimah Fadhil Jaber, Diyah Kammel Shary, Haider Alrudainy
Department of Electrical Power Engineering Techniques, Southern Technical University, Basra, Iraq

Article Info

ABSTRACT

Due to end effects phenomena that cause a decrease of air-gap flux and thrust force, obtaining a precise velocity for a linear induction motor (LIM) has become a significant challenge. This study suggests implementing a novel controller based on a self-recurrent wavelet neural network (SRWNN) and model predictive controller (MPC) to regulate the velocity and thrust force of LIM. The MPC was used to train the SRWNN in this study. The ultimate goal of employing such a control approach in neural network training is to reduce the degree of uncertainty caused by changes in motor parameters and load disturbance. The indirect field-oriented control (IFOC) approach was used to investigate velocity and flux control under varied loading circumstances. Furthermore, to supply the required LIM stator voltage, a SVPWM dependent voltage source inverter was used in this work. To ensure reliable performance, the suggested system combines the benefits of neural networks with the MPC method, resulting in a versatile controller with a basic construction that is easy to accomplish. The MATLAB package is utilized to simulates and outputs LIM responses. The results confirm that the proposed method, which efficiently controls the velocity and thrust force of the LIM, can cope with changes in load force disruption and motor parameters.

Corresponding Author:

Fatimah Fadhil Jaber
Department of Electrical Power Engineering Techniques, Southern Technical University
Basra, Iraq
Email: fatimah.jaber@stu.edu.iq

1. INTRODUCTION

Owing to the benefits that linear induction motor possesses like, low cost, high acceleration/deceleration, low energy consumption, low vibration, there is no requirement for a mechanism to convert rotational motion to translational motion, low noise, easy maintenance, and so on, linear induction motor (LIM) has been extensively utilized in several industrial process and transportation implementations [1], [2]. The LIM's driving principles are identical to the rotary induction motor (RIM) principles, nevertheless the control features of LIM are much more complex as compared to the RIM, furthermore the parameters of the motor vary in time owing to the alteration in operating conditions, including temperature, rail's configurations, and speed of the mover [3], [4]. The key difference between the LIM and the RIM is associated to the end effects that impact the operation and the parameters of the motor under normal state. Therefore, it must be considering in the control and modelling of the LIMs [5]. The drawbacks listed above increase the difficulty of developing a high-grade controller for LIMs. Diverse control groups have currently been used to control the LIM's velocity. Field-orientation control or vector control is the most reliable approach for regulating the speed of the AC motor to achieve superior performance. A complex current is manufactured from two quadrature components in the vector control scheme, one of which is responsible for the motor flux level, and the

other controls the output of force in the motor [6]. In this work, space vector pulse width modulation fed the 3-phase inverter has been used to provide output voltage with good performance and fewer harmonics [7].

Model predictive control is a constrained optimum control method that calculates the optimum control inputs by minimizing a specified objective function over a prediction horizon [8]. As a result, plethora of exploratory research demonstrated that model predictive controller (MPC) can be significantly effective in such processes than the PID controller counterparts [9], [10]. Deep neural networks have revolutionized several fields in recent years. They are increasingly utilized in practical applications and important decision processes, such as innovative knowledge discovery approaches, autonomous driving, or medical image analysis, because to their capacity to naturally learn from structured data and demonstrate better performance [11]. The wavelet neural network (WNN) is one of the most important feedforward neural networks, and it has been the subject of much debate in recent years. The recurrent wavelet neural networks is a more advanced wavelet neural networks model [12], [13].

In this paper, self-recurrent wavelet neural network is employed to control the velocity and thrust force of the linear induction motor. For training the proposed self-recurrent wavelet neural network (SRWNN), the MPC control technique has been used. The reason of using such a control scheme to train the SRWNN is to minimize the impact of load disruptions and to take into account significant modeling uncertainty. The training data has been obtained by modeling the MPC controller for different operating conditions. This data, then, has been adopted in the proposed power system in the face of adjustments in plant parameters and load disruption. This is, consequently, assisted to achieve the required degree of robust output. Using the learning capability of neural networks, the suggested controller is then rebuilt. Under the load disruption and parameters variation, the proposed control technique has been investigated. A comparison has been made between the response of the SRWNN, MPC, and the PID controllers. Simulation outcomes clearly revealed that the postulated scheme can effectively be implemented to control LIM speed with superior outcomes than the counterpart controllers in the literature.

In the recent years, controlling the speed of LIM was studied by a plethora of research papers, as can be seen in Table 1, including the use of enumerative nonlinear MPC [14]. Regardless of its advantages, the use of MPC in combination with a pulse width modulation inverter causes in a high switching frequency at the inverter switches. Furthermore, real-time execution is impossible due to the computing pressure of on-line optimization and linearization. The DTFC approach was analyzed with taking into account the end-effect [15]. DTFC is an improved control technique that uses many PI controllers, but it requires a variable switching frequency and high sampling rate due to hysteresis-based control loops. Bessaih *et al.* [16] proposed speed control design with end effects compensation using rotor time constant estimation is investigated to estimate end effects variation and to obtain a flux and speed tracking objective under load disruption. This scheme, however, is particularly susceptible to changes in the parameters of motor, which differ with saturation of the magnetizing inductance and temperature. Sliding mode control (SMC) was first introduced as a speed control algorithm for LIMs [17].

Table 1. Literature review of approaches used to control LIM

Reference	Approaches	Drive	Advantages	Disadvantages
[14]	MPC	DTC	Easy to implement, robust in the face of load disruption and parameter uncertainty	High switching frequency at the inverter switches
[15]	Several PI controllers	DTFC	Fast dynamic response, very simple, there is no need for a rotor position detector for direct thrust control, and the thrust ripple is low	Hysteresis-based control loops result in a high sampling rate and variable switching frequency
[16]	PI+MRAC	IFOC	Good performances	Sensitive to the variation of the motor parameters which fluctuates with temperature and saturation of the magnetizing inductance
[17]	SMC	DTC	Fast and good speed tracking	Complex design
[18]	SMC+Fuzzy	IFOC	Effective tracking	Very complicated implementations
Proposed	SRWNN+MPC	IFOC	Simple scheme, effective control	

An extended sliding mode load thrust observer (ESO) was then proposed to compensate the sliding mode controller for load thrust disturbances. Moreover, the sliding mode control integrated with ESO is structured to regulate the LIM's speed, flux, and thrust by direct thrust control (DTC) and space-vector modulation (SVM). The sliding mode control's output is utilized as the reference thrust for the direct thrust control, which is dependent upon space-vector modulation (DTC-SVM). Chiang *et al.* [18] proposed an optimized adaptive tracking control for a LIM drive considering the unknown end effects, uncertainties including the friction force and payload. The dynamic model of a field-oriented linear induction motor drive with the end effect of primary is first examined. To deal with the lumped uncertainties of the LIM drive, a

sliding mode controller with a practical fuzzy compensator is designed based on the backstepping control design. Furthermore, an adaptive method based on the sense of the Lyapunov stability theorem is derived to online change the fuzzy compensation gains to solve the difficulty of the unknown bound of the lumped uncertainties in the overall system.

2. LINEAR INDUCTION MOTOR MATHEMATICAL MODEL

Based on the d-q axis electrical circuits the mathematical model of LIM can be built. The LIM's q-axis electrical circuit is the same as the q-axis electrical circuit of a RIM, which means that the parameters are unaffected by the end effects. Nevertheless, the d-axis entry secondary currents influence the flux of the air gap by reducing λ_{dr}. Consequently, where the end effects are considered, the d-axis electrical circuit of the RIM cannot be employed in the LIM study. Figure 1 (a) and Figure 1 (b) demonstrates the d-q axis circuits of LIM when end effects are taking into account [19], [20].
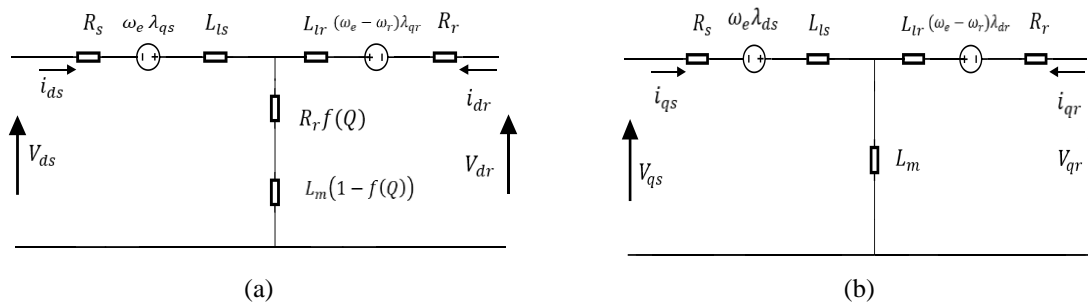

Figure 1. Demonstrates (a) LIM's d-axis electrical circuit (b) LIM's q-axis electrical circuit

Based upon the d-q axis electrical circuit the voltage equations of primary and secondary are described in differential equations in the synchronous reference frame given by [19]:

$$V_{ds} = R_s i_{ds} + R_r f(Q)(i_{ds} + i_{dr}) + p\lambda_{ds} - \omega_e \lambda_{qs} \tag{1}$$

$$V_{qs} = R_s i_{qs} + p\lambda_{qs} + \omega_e \lambda_{ds} \tag{2}$$

$$V_{dr} = R_r i_{dr} + R_r f(Q)(i_{ds} + i_{dr}) + p\lambda_{dr} - \omega_{sl} \lambda_{qr} \tag{3}$$

$$V_{qr} = R_r i_{qr} + p\lambda_{qr} + \omega_{sl} \lambda_{dr} \tag{4}$$

$f(Q)$ is indicated as:

$$f(Q) = \frac{1 - e^{-Q}}{Q} \tag{5}$$

where,

$$Q = \frac{D * R_r}{L_r v} \tag{6}$$

the primary and secondary flux linkages can be described as:

$$\lambda_{ds} = L_{ls} i_{ds} + L_m (1 - f(Q))(i_{ds} + i_{dr}) \tag{7}$$

$$\lambda_{qs} = L_{ls} i_{qs} + L_m (i_{qs} + i_{qr}) \tag{8}$$

$$\lambda_{dr} = L_{lr} i_{dr} + L_m (1 - f(Q))(i_{ds} + i_{dr}) \tag{9}$$

$$\lambda_{qr} = L_{lr} i_{qr} + L_m (i_{qs} + i_{qr}) \tag{10}$$

thrust force:

$$Fe = \frac{3\pi P}{2\tau_p 2}\left(\lambda_{ds}i_{qs} - \lambda_{qs}i_{ds}\right) = M.v' + B.v + F_L \tag{11}$$

where,

V_{ds}, V_{qs} primary voltages in d-q axis (V)
V_{dr}, V_{qr} secondary voltages in d-q axis(V)
i_{ds}, i_{qs} primary currents in d-q axis(A)
i_{dr}, i_{qr} secondary currents in d-q axis(A)
$\lambda_{ds}, \lambda_{qs}$ primary flux linkage in d-q axis
$\lambda_{dr}, \lambda_{qr}$ secondary flux linkage in d-q axis
R_s, R_r primary and secondary resistances (Ω)
L_{ls}, L_{lr} leakage inductances of primary and secondary (H)
L_s, L_r self-inductances of primary and secondary (H)
L_m mutual inductance (H)
P poles number
τ pole pitch (m)
D primary length (m)
Q factor associate with the primary length
V velocity (m/sec)
ω_e angler speed of the primary (rad/sec)
ω_r angler speed of the secondary (rad/sec)
ω_{sl} slip speed (rad/sec)
B   viscous friction (kg/sec)

3.   INDIRECT FIELD-ORIENTED CONTROL OF LIM

The fundamental postulation of the field-oriented control (or called vector control) of LIM is to control the thrust force and flux independently as in DC devices. The secondary flux linkage axis is forced to align with the d-axis in the ideal IFOC, thus [21], [22]:

$$\lambda_{qr} = \frac{d\lambda_{qr}}{dt} = 0 \tag{12}$$

$$\lambda_{dr} = \lambda_r = constant \tag{13}$$

using the IFOC approach and taking into account that the electrical time constant is greatly less than the mechanical time constant. The thrust force equation demonstrated in (11) can be sensibly signified through the equation shown below:

$$F_e = k_f.i_{qs} \tag{14}$$

where,

$$k_f = \frac{3\pi}{2\tau_p} P \frac{L_m(1-f(Q))}{L_r - L_m f(Q)} \lambda_{dr} \tag{15}$$

furthermore, by utilizing equation (3), the slip velocity is given by:

$$V_{sl} = \frac{\tau_p.L_m(1-f(Q)).i_{qs}^*}{\pi(\frac{L_r}{R_r} - \frac{L_m f(Q)}{R_r})\lambda_{dr}} \tag{16}$$

while the equation below defined the electrical velocity as:

$$V_e = V_{sl} + V_r \tag{17}$$

the control method by decoupling employing double current controllers (one for the i_{ds} and the other for i_{qs}), that used to give the required voltages to the space vector pulse width modulation inverter is specified as:

$$V_{ds}^* = \left(k_p\, e(t) + k_i \int_0^t e(t)dt + K_d \frac{de(t)}{dt}\right)(i_{ds}^* - i_{ds}) - \frac{\pi}{\tau_p} V_e L_\sigma(Q) i_{qs}^* \tag{18}$$

$$V_{qs}^* = \left(k_p\, e(t) + k_i \int_0^t e(t)dt + K_d \frac{de(t)}{dt}\right)(i_{qs}^* - i_{qs}) + \frac{\pi}{t_p} V_e L_\sigma(Q) i_{ds}^* + \frac{P.L_m\pi}{L_r\tau_p} V_r \lambda_{dr} \tag{19}$$

where $L_\sigma(Q)$ denotes the leakage inductance represented by:

$$L_\sigma(Q) = L_S - L_m f(Q) - \frac{\left(L_m(1-f(Q))\right)^2}{L_r - L_m f(Q)} \tag{20}$$

4. VOLTAGE SOURCE INVERTER BASED ON SVPWM

A 3-phase voltage source inverter (VSI) is employed to give the necessary frequency and voltage to the 3-phase LIM according to the control technique. The SVPWM mechanism is applied to control the 3-phase VSI via providing the essential switching signal. The SVPWM method is derived from the PWM method for a 3-phase inverter via the representation of the space vector in α-β plane. The α-β components are found by Clark's transformation. The major principle of space vector PWM relies on the different switching sequences of the 3-phase VSI. The switches combination can be represented as binary codes that correspond to the power transistor of the 3-phase inverter [23]. Table 2 indicates the possible eight-state switch of the inverter. Six non-zero (active) voltage vectors and two zero (inactive) voltage vectors are probable as a result of switching states as seen in Figure 2, six active voltage vectors (V_1-V_6) form the axes of a hexagonal with a 60° apart between either two neighboring active vectors [24], [25].

Table 2. Demonstrates line to line voltages, phase voltages, and switching vectors

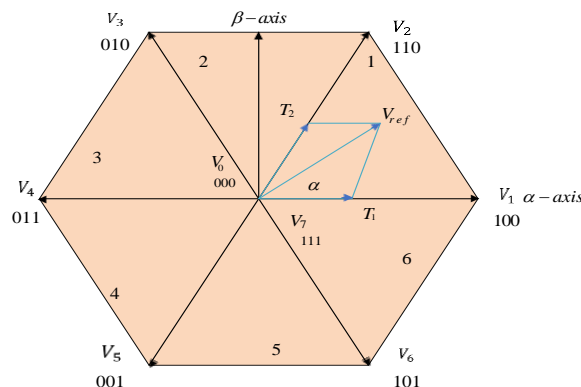| Switching vectors			Phase voltage			The line voltage			Voltage vector
a	b	c	V_a	V_b	V_c	V_{ab}	V_{bc}	V_{ca}	
0	0	0	0	0	0	0	0	0	V_0
1	0	0	$\frac{2V_{dc}}{3}$	$-\frac{V_{dc}}{3}$	$-\frac{V_{dc}}{3}$	V_{dc}	0	$-V_{dc}$	V_1
1	1	0	$\frac{V_{dc}}{3}$	$\frac{V_{dc}}{3}$	$-\frac{2V_{dc}}{3}$	0	V_{dc}	$-V_{dc}$	V_2
0	1	0	$-\frac{V_{dc}}{3}$	$\frac{2V_{dc}}{3}$	$-\frac{V_{dc}}{3}$	$-V_{dc}$	V_{dc}	0	V_3
0	1	1	$-\frac{2V_{dc}}{3}$	$\frac{V_{dc}}{3}$	$\frac{V_{dc}}{3}$	$-V_{dc}$	0	V_{dc}	V_4
0	0	1	$-\frac{V_{dc}}{3}$	$\frac{V_{dc}}{3}$	$\frac{2V_{dc}}{3}$	0	$-V_{dc}$	V_{dc}	V_5
1	0	1	$\frac{V_{dc}}{3}$	$-\frac{2V_{dc}}{3}$	$\frac{V_{dc}}{3}$	V_{dc}	$-V_{dc}$	0	V_6
1	1	1	0	0	0	0	0	0	V_7

Figure 2. Shows switching and voltage vectors

5. MODEL PREDICTIVE CONTROL

Since it is a conventional nonlinear control method in process industries such as petrochemical industries, model predictive control is becoming an emerging control approach in the domains of power

electronics and electric drives [26]. The MPC framework depends upon the explicit usage of the system's response forecast model to obtain control behavior via minimalizing the objective function. Minimization of the difference between the expected and reference response, as well as control effort exposed to prescribed constraints, are among the optimization objectives. The efficacy of the MPC has been verified to be equal to optimum control. At every control interval, the first input in the optimal series is delivered into the plant, and the entire computation is repeated at later control times. The objective of capturing new measurements at each stage of the process is to correct for model inaccuracies and unmeasured disruptions, which all result in the system's output being different from what the model predicted [27]-[29].

A basic model predictive control configuration is demonstrated in Figure 3. The internal model is utilized to forecast the future outcomes of the plant depends upon the inputs and outputs' past and present values and the suggested optimum future control actions. There are two key components of the prediction, the free response, which is the predicted output behavior based on the assumption that there are no future control actions, and the extra part named the forced response owing to a precalculated set of future actuating values. The entire forecast can be determined for linear systems by summing up forced and free responses, the target value that the output must be achieved is called the reference trajectory signal. The optimizer calculates the best range of possible control actions by reducing the cost function J, and the optimization is subjected to constraints on manipulated and controlled variables [30].

The ultimate goal is to reduce future output error to zero with minimal input effort. In general, the cost function to be minimalized, such as in generalized predictive control, is a weighted sum of predicted square errors and future square control values [30].

$$J(N_1, N_2, N_u) = \sum_{j=N_1}^{N_2} \beta(j)[y^\wedge(k+j|k) - w(k+j)]^2 + \sum_{j=1}^{N_u} \lambda(j)[u(k+j-1)]^2 \qquad (21)$$

Where N_1 and N_2 signifies the lower and upper prediction horizon, $\lambda(j) and \beta(j)$ represents the weighting factors, and N_u specifies the control horizon. Depending on the relationship below, the control horizon enables for a reduction in the calculated future control number.

$$\Delta u(k+j) = 0 \ for \ j \geq N_u \qquad (22)$$

$w(k+j)$ signifies the reference trajectory over the future control N. Constraints on the outputs, inputs and the control signal changing may be applied to the cost function.

$$u_{min} \leq u(k) \leq u_{max} \qquad (23)$$

$$\Delta u_{min} \leq \Delta u(k) \leq \Delta u_{max} \qquad (24)$$

$$y_{min} \leq y(k) \leq y_{max} \qquad (25)$$

When the given constraints in (23)-(25) are met, solution of (21) gives the optimum control signal sequences over the horizon.
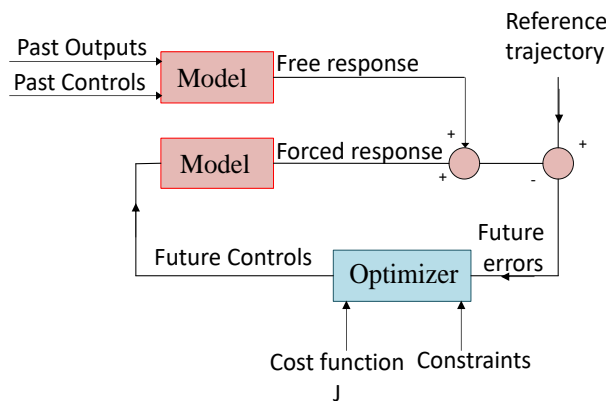

Figure 3. Illustrates MPC's fundamental structure

6. ADAPTIVE FORECASTING MODEL BY SRWNN

To achieve a better approximate performance of the artificial neural networks (ANNs), a wavelet neural network (WNNs) was formed via a mixture of the neural networks with the wavelets. WNNs are feed-forward neural networks that use wavelets instead of sigmoid activation as the activation function. One or more inputs may be used in WNNs, with one hidden layer and one or more outputs. The hidden layers of WNNs consist of many neurons with wavelet activation functions rather than sigmoid functions. To achieve adaptive WNN, the parameters of the WNNs (weights, translation, and dilation factors) are optimized using any learning algorithm. It can divide the wavelet neural networks into feedforward (non-recurrent) and recurrent groups [31].

In this work, the SRWNN is used to control the thrust force and velocity of the linear induction motor. The structure of SRWNN is shown in Figure 4. It consists of four layers. The first layer accepts multiple M-signaled input signals from the outside and sends them directly to the hidden layer's (second layer). A wavelon is a node in the hidden layer (shown by a dashed box) that is made up of neurons that are proportionate to the number of input elements, meaning that every neuron in each wavelon corresponds to one element in the input vector. Each neuron in the wavelon is described by a mother wavelet function and self-feedback loop. In this study, the first derivative of a Gaussian function was employed as an activation function, which was denoted as [32]:

$$\emptyset(x) = -x \, exp(\frac{-x^2}{2}) \tag{26}$$

from its mother wavelet, the output of any neuron $\emptyset_{ij}(k)$ present in either wavelon is obtained as follows:

$$\emptyset_j\left(z_{ij}(k)\right) = \emptyset(\frac{u_{ij}(k) - t_{ij}(k)}{\lambda_{ij}(k)}) \tag{27}$$

with

$$z_{ij}(k) = \frac{u_{ij}(k) - t_{ij}(k)}{\lambda_{ij}(k)} \tag{28}$$

The first subscript i denotes the position of the wavelon, while the second subscript j denotes the location of the neuron inside that wavelon. It's worth noticing that the subscript for the location of the input signal $u_j(k)$ is the same as the subscript for the position of the neuron. The values of the translation and dilation variables are represented by the expressions $t_{ij}(k)$ and $\lambda_{ij}(k)$, respectively. In addition, every neuron's input signal is composed of the signal from the input layer plus the delayed weighted output of its unit, i.e.

$$u_j(k) = x_j(k) + w_{ij}^D(k)\phi_{ij}(k-1) \tag{29}$$

The $w_{ij}^D(k)$ symbol is used here to represents the weighted self-feedback loop (as illustrated in Figure 4 by a blue arrow in the second layer). In a multidimensional SRWNN (M > 1), the total output of each wavelon is equal to the product of the outputs of each of its neurons. This product operation is performed at the third layer and for each hidden wavelon, it is calculated as follows:

$$\psi_i(k) = \prod_{j=1}^{M} \left\{ -\left[\frac{u_j(k) - t_{ij}(k)}{\lambda_{ij}(k)} \right] \right\} \times \left\{ exp\left[-\frac{1}{2}\left(\frac{u_j(k) - t_{ij}(k)}{\lambda_{ij}(k)} \right)^2 \right] \right\} \tag{30}$$

Figure 4 shows a weighted relationship between the input signals and the output neuron(s), $a_j(k)$ is utilized to describe these weights. And these input signals weights summation $\sum_{j=1}^{M} x_j(k)a_j(k)$, is termed as a direct term. By employing this direct term, the SRWNN gains the advantages of a direct linear feed-through network, such as increased extrapolation outside of examples of learning data sets and network parameter initialization based on available plant information. The SRWNN becomes a WNN when the self-feedback loop's weights and all $(a_j(k))$ weights are set to zero. Finally, the fourth layer is referred to as the output layer. Its induced field is equal to the weighted sum of the third layer's outputs plus the weighted sum of the input values of the first layer. SRWNN's output is the result of this complete process. Hence,

$$Y_{SRWNN}(k) = \sum_{i=1}^{R} w_i^0(k)\psi_i(k) + \sum_{j=1}^{M} x_j(k)a_j(k), \tag{31}$$

where the fourth- and third-layers' connection weights are denoted by $w_i^0(k)$. The adjustable parameters of SRWNN are as follows:

$$P_I = \{a_j(k), w_j^0(k), w_{ij}^D(k), t_{ij}(k), \lambda_{ij}(k)\} \tag{32}$$

finally, we will alter the various parameters of SRWNN using a dynamic backpropagation approach based on the gradient descent technique.

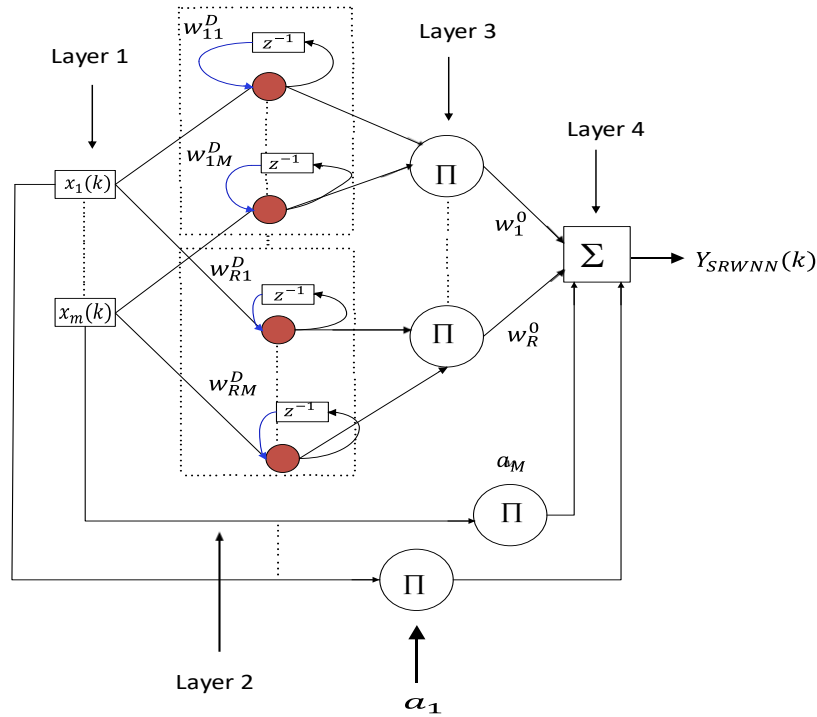Figure 4. Shows the SRWNN structure

7.   SYSTEM CONFIGURATION

Figure 5 displays the block diagram of a LIM drive based upon an indirect field orientation. It is composed of LIM, coordinate translators, VSI, current controller, and IFOC mechanism. For the calculation and supply of the speed signal necessary for closed-loop control, a linear speed sensor was used. To get the force current component i_{qs}^*, the calculated speed is compared to the reference speed and its difference is fed to the SRWNN controller, while i_{ds}^* is set at the rated quantity. The i_{qs}^* and i_{ds}^* are utilized to get the slip according to equation (16). This latter is combined with the measured speed and integrated the sum to achieve the field angle θ_e. The reference value of quadrature current of the primary (i_{qs}^*) for the current controller that is then compared with the feedback current (i_{qs}) from the motor to get the essential voltage V_q for the SVPWM inverter for regulatory the thrust force. While we can control the flux via the current controller to control the d-axis current (i_{ds}), by comparing it to the reference current (i_{ds}^*), to get the required voltage V_d. Using the IFOC method the transfer function of LIM can be drive from (11) as:

$$Transfer\ Functiom = \frac{V}{F_e - F_L} = \frac{1}{Ms + B} \tag{33}$$

the simplified linearized LIM model defined by (33) is utilized in the MPC controller structure which is used for the off-line training of the proposed SRWNN controller for fast implantation, as seen in Figure 6.
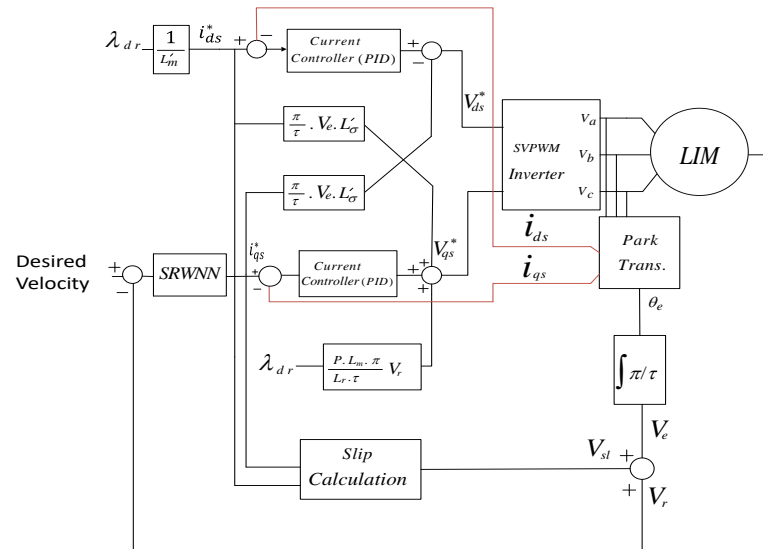
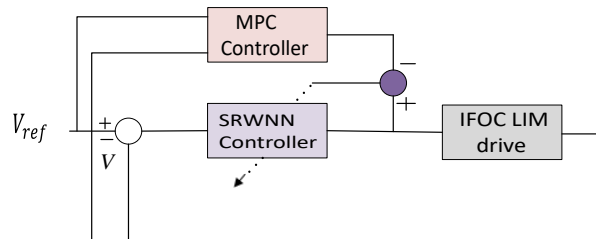Figure 5. Represents proposed block diagram of IFOC for LIM

Figure 6. Illustrates the proposed scheme of MPC based SRWNN controller

8.   SIMULATION RESULTS

To emphasis the feasibility of the suggested scheme, an extensive simulation study has been carried out in this study. To this end, the MATLAB/SIMULINK toolbox kit has been used in this work. In this work, an extensive parametric analysis of MPC has been investigated to set the optimum values of the controller as shown in Figures 7 and 8.

Firstly, the control horizon and weight on output is fixed as 40, and 100, respectively. This is because they have a lower impact on the response of the controller, therefore these parameters are considered constant. Then, the prediction horizon is varied from 5 to 100, and sample time is varied from 0.00005 to 0.01 sec. Consequently, the impact of these variations on the settling time and rising time are plotted as can be illustrated in Figures 7 and 8. Therefore, in this study, the MPC parameters which has been used in our proposed scheme are chosen, based on our extensive investigation, as shown in Table 3. Table 4 demonstrate the LIM parameters used in this work.
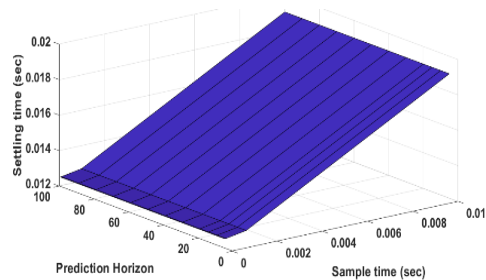
Figure 7. Demonstrate the influence of prediction horizon and sampling time variations on the settling time
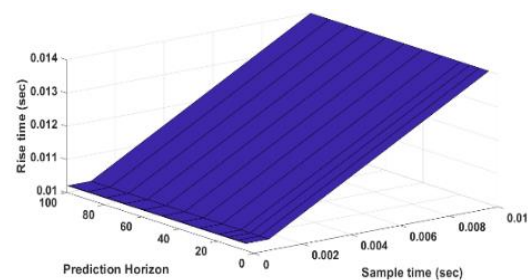
Figure 8. Demonstrate the influence of prediction horizon and sampling time variations on the rising time

Table 3. Optimum MPC parameters based on our parametric analysis

Prediction horizon	Control horizon	Weights on manipulated variables	Weights on manipulated variable rates	Weights on the output signals	Sampling interval
65	40	0	0.019	100	0.00005

The force generated and the motor's velocity are both constrained as:

Max. thrust force = 1500 N

Min. thrust force = 210 N

Max. speed of the mover= 4 m/sec

Min. speed of the mover = 0 m/sec

The SRWNN controller parameters are:

The speed input error (e_V = Desired Speed- Measured Speed)

Output is i_{qs}^*

Mean square error (MSE) of SRWNN= 1.6301e-5

Table 4. Parameters used in the linear induction motor model

Parameters	values
P	4
τ_p (m)	0.0465
$R_s(\Omega)$	13.2
$R_r(\Omega)$	11.78
$L_s(H)$	0.42
$L_r(H)$	0.42
$L_m(H)$	0.4
M(kg)	4.775
B(kg/m)	53

Through performing several experiments along with several separate operation scenarios, the effectiveness of the current controller for regulating the LIM velocity was attained. This involves the velocity response in the case of no-load and a rapid variation in the load at the reference velocity. The response of the velocity at no load and a sudden load of 200N at 0.5 sec with reference velocity 4(m/sec) is demonstrated in Figure 9. The developed thrust force during no-load and load (200 N at 0.5 sec) is demonstrated in Figure 10. Another change of load force by amount of 300 N is applied on the motor at 0.5 sec, the velocity and thrust force of LIM at this load is displayed in Figure 11 and Figure 12, respectively. Figure 13 and Figure 14 displayed the step changed in load for velocity and force respectively (100 N at 0.2 sec and 200 N at o.5 sec). Figure 15 demonstrated the velocity response at variation of parameters (increase R_r by 25% and M by 50% in the model of the motor only) with load condition of 200 N. Finally, comparation between the responses of velocity using traditional PID, MPC, and SRWNN is demonstrated in Figure 16.
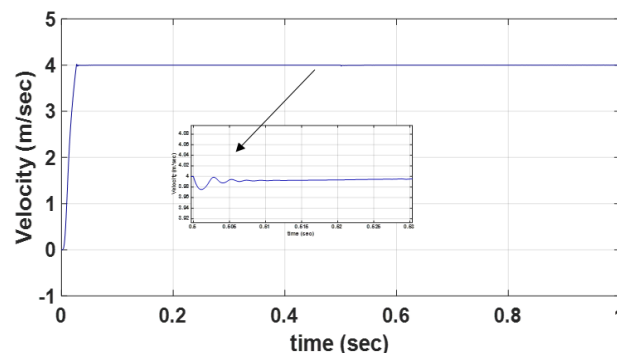

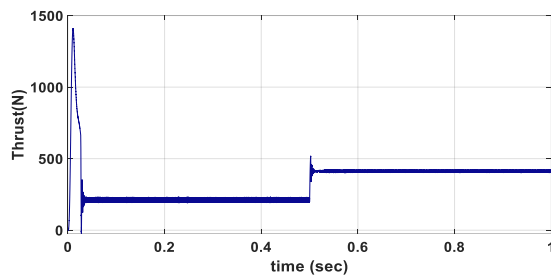Figure 9. Velocity response under load disruption (200N)

Figure 10. The developed LIM thrust force under load disruption (200 N)
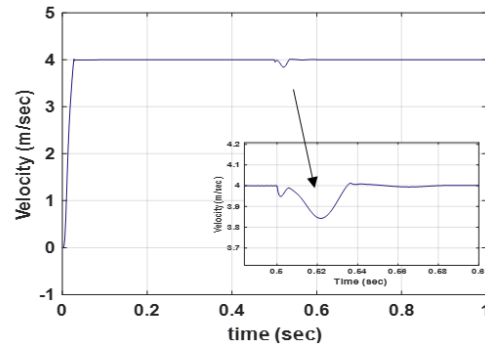

Figure 11. Velocity response under load disruption (300N)
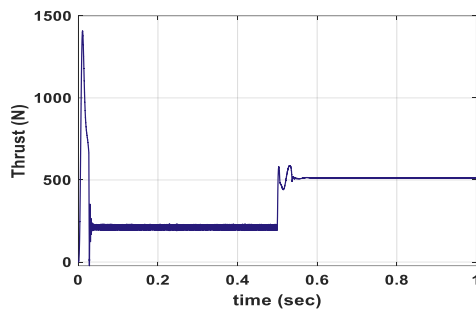

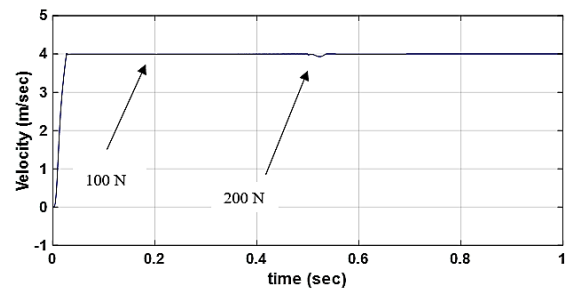Figure 12. The developed LIM thrust force under load disruption (300N)

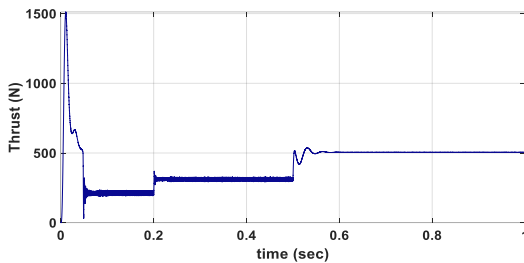Figure 13. Velocity response under step change of load

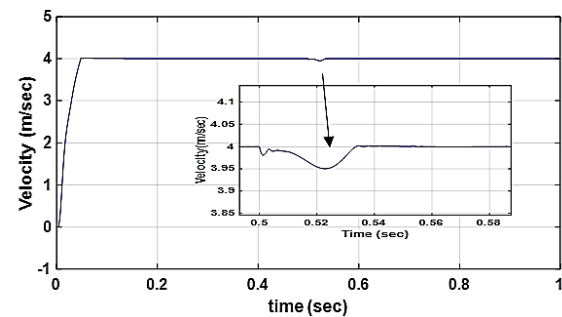Figure 14. Thrust force under step change of load

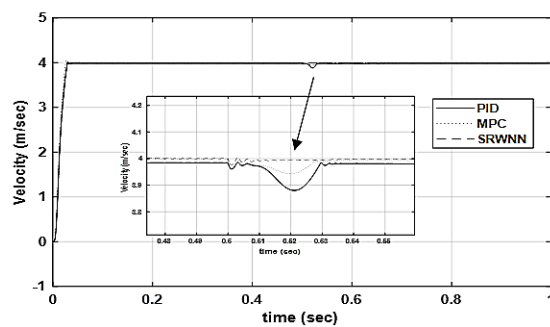Figure 15. Velocity response under change of load and parameters variation

Figure 16. Comparison between the responses of the speed of LIM by MPC, PID, and SRWNN at load 200 N

9.   CONCLUSION

The SRWNN has been used to control the thrust force and velocity of linear induction motor in this study. The velocity control issue is initially developed as an optimization control problem using the MPC approach, after that, samples produced from the application of the MPC controller to the indirect field-oriented LIM drive under load changes and varied operating circumstances are used to train the proposed SRWNN controller. Via load force disruption and mismatched parameters, the suggested controller has been investigated. The simulation results showed that the proposed controller was viable under various loading states.

REFERENCES

[1]   C. RAJA and K. R. Sudha, "Optimal design of equivalent linear induction motor based on harmony search algorithm and analysis using finite element method," *Journal of Engineering Science and Technology,* vol. 13, no. 8, pp. 2520-2532, 2018.
[2]   D. Xu, J. Huang, X. Su, and P. Shi, "Adaptive command-filtered fuzzy backstepping control for linear induction motor with unknown end effect," *Information Sciences,* vol. 477, pp. 118-131, 2019, doi: 10.1016/j.ins.2018.10.032.
[3]   I. Bouserhane, A. Boucheta, A. Hazzab, B. Mazari, and P. Sicard, "Adaptive backstepping controller design for linear induction motor position control," in *AIP Conference Proceedings*, vol. 1107, no. 1, p. 126, 2009, doi: 10.1063/1.3106460.
[4]   Y. Han, Z. Nie, J. Xu, J. Zhu, and J. Sun, "Control strategy for optimising the thrust of a high-speed six-phase linear induction motor," *IET Power Electronics,* vol. 13, no. 11, pp. 2260-2268, 2020, doi: 10.1049/iet-pel.2019.1334.
[5]   A. L. Saleh, B. A. Obaid, and A. A. Obed, "Motion control of linear induction motor based on optimal recurrent wavelet neural network-PID controller," *International Journal of Engineering & Technology,* vol. 7, no. 4, pp. 2028-2034, 2018.
[6]   M. Aktas, K. Awaili, M. Ehsani, and A. Arisoy, "Direct torque control versus indirect field-oriented control of induction motors for electric vehicle applications," *Engineering Science and Technology, an International Journal,* vol. 23, no. 5, pp. 1134-1143, 2020, doi: 10.1016/j.jestch.2020.04.002.
[7]   S. R. Karchung, "Open-Loop Vector Control of Induction Motor with Space Vector Pulse Width Modulation Technique," *Int. J. Electr. Comput. Eng.,* vol. 13, no. 9, pp. 618-623, 2019, doi: 10.5281/zenodo.3461968.
[8]   J. Drgoňa *et al.*, "All you need to know about model predictive control for buildings," *Annual Reviews in Control*, vol. 50. pp. 190-132, 2020, doi: 10.1016/j.arcontrol.2020.09.001.
[9]   F. M. Salem, M. I. Mosaad, and M. A. Awadallah, "A comparative study of MPC and optimised PID control," *International Journal of Industrial Electronics and Drives,* vol. 2, no. 4, pp. 242-250, 2015, doi: 10.1504/IJIED.2015.076293.
[10]   N. Mohammad, A. Azman, M. Marzaki, R. Adnan, N. Ismail, and M. Rahiman, "Comparison between MPC and PID control for compact hydro distillation process," *Journal of Fundamental and Applied Sciences,* vol. 9, no. 4S, pp. 77-93, 2017, doi: 10.4314/jfas.v9i4S.5.
[11]   M. Alber *et al.*, "iNNvestigate neural networks!," *Arxiv*, 2018. [Online] available: https://arxiv.org/abs/1808.04260
[12]   L. Huang and J. Wang, "Forecasting energy fluctuation model by wavelet decomposition and stochastic recurrent wavelet neural network," *Neurocomputing,* vol. 309, pp. 70-82, 2018, doi: 10.1016/j.neucom.2018.04.071.
[13]   M. H. Hamedani, M. Zekri, and F. Sheikholeslam, "Adaptive impedance control of uncertain robot manipulators with saturation effect based on dynamic surface technique and self-recurrent wavelet neural networks," *Robotica,* vol. 37, no. 1, pp. 161-188, 2019, doi: 10.1017/S0263574718000930.
[14]   J. Thomas and A. Hansson, "Speed Tracking of a Linear Induction Motor-Enumerative Nonlinear Model Predictive Control," *IEEE Transactions on Control Systems Technology*, vol. 21, no. 5, pp. 1956-1962, Sept. 2013, doi: 10.1109/TCST.2012.2217745.
[15]   H. Shadabi, A. R. Sadat, A. Pashaei, and M. Sharifian, "Speed Control of Linear Induction Motor Using DTFC Method Considering end-effect Phenomenon," *International Journal on Technical and Physical Problems on Engineering,* vol. 6, no. 4, pp. 75-81, 2014.
[16]   B. Bessaih, A. Boucheta, I. K. Bousserhane, A. Hazzab and P. Sicard, "Speed control of linear induction motor considering end-effects compensation using rotor time constant estimation," *International Multi-Conference on Systems, Signals & Devices*, 2012, pp. 1-7, doi: 10.1109/SSD.2012.6197999.
[17]   M. M. Ali, W. Xu, M. F. Elmorshedy, Y. Liu, S. M. Allam and M. Dong, "Sliding Mode Speed Regulation of Linear Induction Motors Based on Direct Thrust Control with Space-Vector Modulation Strategy," *2019 22nd International Conference on Electrical Machines and Systems (ICEMS)*, 2019, pp. 1-6, doi: 10.1109/ICEMS.2019.8921938.
[18]   H. Chiang, K. Hsu and I. Li, "Optimized Adaptive Motion Control Through an SoPC Implementation for Linear Induction Motor Drives," in *IEEE/ASME Transactions on Mechatronics*, vol. 20, no. 1, pp. 348-360, Feb. 2015, doi: 10.1109/TMECH.2014.2313594.
[19]   A. L. Saleh *et al.*, "Anti-windup scheme based on 2DOF-PIλDμ controller for velocity tracking of linear induction motor," *International Transactions on Electrical Energy Systems,* vol. 29, no. 12, p. e12134, 2019, doi: https://doi.org/10.1002/2050-7038.12134.
[20]   L. Lu, P. Sun, L. Xu, and M. Luo, "Adaptive robust motion control for linear induction motor with electromagnetic nonlinearity compensation," *Asian Journal of Control,* vol. 21, no. 5, pp. 2441-2450, 2019, doi: 10.1002/asjc.1843.
[21]   O. Mahmoudi and A. Boucheta, "Adaptive integral backstepping controller for linear induction motors," *Int J Pow Elec & Dri Syst,* vol. 10, no. 2, pp. 709-719, 2019, doi: 10.11591/ijpeds.v10.i2.pp709-719.
[22]   A. Boucheta, I. Bousserhane, A. Hazzab, P. Sicard, and M. Fellah, "Speed control of linear induction motor using sliding mode controller considering the end effects," *Journal of Electrical Engineering and Technology,* vol. 7, no. 1, pp. 34-45, 2012, doi: 10.5370/JEET.2012.7.1.34.
[23]   T. A. Hussein and L. A. Mohammed, "Detailed Simulink implementation for induction motor control based on space vector pulse width modulation SVPWM," *Indonesian Journal of Electrical Engineering and Computer Science,* vol. 22, no. 3, pp. 1251-1262, 2021, doi: 10.11591/ijeecs.v22.i3.pp1251-1262.
[24]   W. Wang *et al.*, "New Three-Phase Current Reconstruction for PMSM Drive With Hybrid Space Vector Pulsewidth Modulation Technique," *IEEE Transactions on Power Electronics*, vol. 36, no. 1, pp. 662-673, Jan. 2021, doi: 10.1109/TPEL.2020.2997986.
[25]   M. Yusuf, V. Prasetia, S. D. Riyanto, and A. A. Rafiq, "Simulation Design of Speed Control of Three Phase Induction Motors with Switching Space Vector Pulse Width Modulation," *Jurnal Ecotipe (Electronic, Control, Telecommunication, Information, and Power Engineering),* vol. 6, no. 1, pp. 24-31, 2019, doi: 10.33019/ecotipe.v6i1.943.

[26] F. Wang, X. Mei, J. Rodriguez and R. Kennel, "Model predictive control for electrical drive systems-an overview," *CES Transactions on Electrical Machines and Systems*, vol. 1, no. 3, pp. 219-230, September 2017, doi: 10.23919/TEMS.2017.8086100.

[27] S. M. Akbar, A. Hasan, A. J. Watson and P. Wheeler, "Model Predictive Control With Triple Phase Shift Modulation for a Dual Active Bridge DC-DC Converter," *IEEE Access*, vol. 9, pp. 98603-98614, 2021, doi: 10.1109/ACCESS.2021.3095553.

[28] I. S. Mohamed, S. Rovetta, T. D. Do, T. Dragicević and A. A. Z. Diab, "A Neural-Network-Based Model Predictive Control of Three-Phase Inverter With an Output \$LC\$ Filter," *IEEE Access*, vol. 7, pp. 124737-124749, 2019, doi: 10.1109/ACCESS.2019.2938220.

[29] S. J. Qin and T. A. Badgwell, "A survey of industrial model predictive control technology," *Control engineering practice,* vol. 11, no. 7, pp. 733-764, 2003, doi: 10.1016/S0967-0661(02)00186-7.

[30] A. A. Zaki Diab, D. A. Kotin, V. N. Anosov and V. V. Pankratov, "A comparative study of speed control based on MPC and PI-controller for Indirect Field oriented control of induction motor drive," *2014 12th International Conference on Actual Problems of Electronics Instrument Engineering (APEIE)*, 2014, pp. 728-732, doi: 10.1109/APEIE.2014.7040781.

[31] A. L. Saleh *et al.*, "Wavelet Neural Networks for Speed Control of BLDC Motor", in Automation and Control. London, United Kingdom: IntechOpen, 2020 [Online]. Available: https://www.intechopen.com/chapters/71323 doi: 10.5772/intechopen.91653

[32] R. Kumar, S. Srivastava, J. Gupta, and A. Mohindru, "Self-recurrent wavelet neural network–based identification and adaptive predictive control of nonlinear dynamical systems," *International Journal of Adaptive Control and Signal Processing,* vol. 32, no. 9, pp. 1326-1358, 2018, doi: 10.1002/acs.2916.

BIOGRAPHIES OF AUTHORS

Fatimah Fadhil Jaber received a Bachelor's degree in Electrical Power Engineering Techniques. Master's student in Electrical Power Engineering Techniques, specializing in Power and Machine. She can be contacted at email: Fatimah.jaber@stu.edu.iq.

Diyah Kammel Shary is bachelor's degree in Electrical Engineering, Master's in Electrical Engineering-Power and Machines, PhD in Electrical Engineering-Power and Machinery from the University of Basra. He can be contacted at email: diyahpower@stu.edu.iqis.

Haider Alrudainy received both the BSc degrees in electrical engineering from Basra University in Basra/Iraq in 2008 and MSc degree (Hons) in control engineering from Basra university in Basra/Iraq in 2010. He joined his PhD program in the School of Electrical and Electronic Engineering, Newcastle University/UK. He has an interest in exploring cutting-edge computing systems using novel architectures, efficient algorithms and emerging technologies, including many core system, emerging interconnects, VLSI circuits design. He can be contacted at email: h.m.a.alrudainy@stu.edu.iq.